# Search for $\boldsymbol{\nu_\mu} \rightarrow \boldsymbol{\nu_e}$ oscillations in the NOMAD experiment

## NOMAD Collaboration

P. Astier [n], D. Autiero [h], A. Baldisseri [r], M. Baldo-Ceolin [m],
M. Banner [n], G. Bassompierre [a], K. Benslama [i], N. Besson [r],
I. Bird [h,i], B. Blumenfeld [b], F. Bobisut [m], J. Bouchez [r], S. Boyd [t],
A. Bueno [c,x], S. Bunyatov [f], L. Camilleri [h], A. Cardini [j],
P.W. Cattaneo [o], V. Cavasinni [p], A. Cervera-Villanueva [h,v],
R. Challis [k], A. Chukanov [f], G. Collazuol [m], G. Conforto [h,u,1],
C. Conta [o], M. Contalbrigo [m], R. Cousins [j], D. Daniels [c],
H. Degaudenzi [i], T. Del Prete [p], A. De Santo [h,p], T. Dignan [c],
L. Di Lella [h], E. do Couto e Silva [h], J. Dumarchez [n], M. Ellis [t],
G.J. Feldman [c], R. Ferrari [o], D. Ferrère [h], V. Flaminio [p],
M. Fraternali [o], J.-M. Gaillard [a], E. Gangler [h,n], A. Geiser [e,h],
D. Geppert [e], D. Gibin [m], S. Gninenko [h,l], A. Godley [s],
J.-J. Gomez-Cadenas [h,v], J. Gosset [r], C. Gößling [e],
M. Gouanère [a], A. Grant [h], G. Graziani [g], A. Guglielmi [m],
C. Hagner [r], J. Hernando [v], D. Hubbard [c], P. Hurst [c], N. Hyett [k],
E. Iacopini [g], C. Joseph [i], F. Juget [i], N. Kent [k], M. Kirsanov [l],
O. Klimov [f], J. Kokkonen [h], A. Kovzelev [l,o], A. Krasnoperov [a,f],
D. Kustov [f], S. Lacaprara [m], C. Lachaud [n], B. Lakić [w],
A. Lanza [o], L. La Rotonda [d], M. Laveder [m],
A. Letessier-Selvon [n], J.-M. Levy [n], L. Linssen [h], A. Ljubičić [w],
J. Long [b], A. Lupi [g], A. Marchionni [g], F. Martelli [u],
X. Méchain [r], J.-P. Mendiburu [a], J.-P. Meyer [r], M. Mezzetto [m],
S.R. Mishra [c,s], G.F. Moorhead [k], D. Naumov [f], P. Nédélec [a],
Yu. Nefedov [f], C. Nguyen-Mau [i], D. Orestano [q], F. Pastore [q],
L.S. Peak [t], E. Pennacchio [u], H. Pessard [a], R. Petti [h,o],
A. Placci [h], G. Polesello [o], D. Pollmann [e], A. Polyarush [l],
B. Popov [f,n], C. Poulsen [k], L. Rebuffi [m], R. Renò [p], J. Rico [x],
P. Riemann [e], C. Roda [h,p], A. Rubbia [h,x], F. Salvatore [o],
K. Schahmaneche [n], B. Schmidt [e,h], T. Schmidt [e], A. Sconza [m],

M. Sevior [k], D. Sillou [a], F.J.P. Soler [h,t], G. Sozzi [i], D. Steele [b,i],
U. Stiegler [h], M. Stipčević [w], Th. Stolarczyk [r], M. Tareb-Reyes [i],
G.N. Taylor [k], V. Tereshchenko [f], A. Toropin [l],
A.-M. Touchard [n], S.N. Tovey [h,k], M.-T. Tran [i], E. Tsesmelis [h],
J. Ulrichs [t], L. Vacavant [i], M. Valdata-Nappi [d,y],
V. Valuevcorr [f,j], [corr] Corresponding author.
Slava.Valouev@cern.ch F. Vannucci [n], K.E. Varvell [t], M. Veltri [u],
V. Vercesi [o], G. Vidal-Sitjes [h], J.-M. Vieira [i], T. Vinogradova [j],
F.V. Weber [c,h], T. Weisse [e], F.F. Wilson [h], L.J. Winton [k],
B.D. Yabsley [t], H. Zaccone [r], K. Zuber [e], P. Zuccon [m]

[a] *LAPP, Annecy, France*
[b] *Johns Hopkins Univ., Baltimore, MD, USA*
[c] *Harvard Univ., Cambridge, MA, USA*
[d] *Univ. of Calabria and INFN, Cosenza, Italy*
[e] *Dortmund Univ., Dortmund, Germany*
[f] *JINR, Dubna, Russia*
[g] *Univ. of Florence and INFN, Florence, Italy*
[h] *CERN, Geneva, Switzerland*
[i] *University of Lausanne, Lausanne, Switzerland*
[j] *UCLA, Los Angeles, CA, USA*
[k] *University of Melbourne, Melbourne, Australia*
[l] *Inst. for Nuclear Research, INR Moscow, Russia*
[m] *Univ. of Padova and INFN, Padova, Italy*
[n] *LPNHE, Univ. of Paris VI and VII, Paris, France*
[o] *Univ. of Pavia and INFN, Pavia, Italy*
[p] *Univ. of Pisa and INFN, Pisa, Italy*
[q] *Roma Tre University and INFN, Rome, Italy*
[r] *DAPNIA, CEA Saclay, France*
[s] *Univ. of South Carolina, Columbia, SC, USA*
[t] *Univ. of Sydney, Sydney, Australia*
[u] *Univ. of Urbino, Urbino, and INFN Florence, Italy*
[v] *IFIC, Valencia, Spain*
[w] *Rudjer Bošković Institute, Zagreb, Croatia*
[x] *ETH Zürich, Zürich, Switzerland*
[y] *Now at Univ. of Perugia and INFN, Italy*

We present the results of a search for $\nu_\mu \to \nu_e$ oscillations in the NOMAD experiment at CERN. The experiment looked for the appearance of $\nu_e$ in a predominantly $\nu_\mu$ wide-band neutrino beam at the CERN SPS. No evidence for oscillations was found. The 90% confidence limits obtained are $\Delta m^2 < 0.4$ eV$^2$ for maximal mixing and $\sin^2(2\theta) < 1.4 \times 10^{-3}$ for large $\Delta m^2$. This result excludes the LSND allowed region of oscillation parameters with $\Delta m^2 \gtrsim 10$ eV$^2$.

# 1 Introduction

The NOMAD experiment was designed to search for $\nu_\tau$ appearance from neutrino oscillations in the CERN wide-band neutrino beam produced by the 450 GeV proton synchrotron (SPS). The detector was optimized to identify efficiently electrons from $\tau^- \to e^- \bar{\nu}_e \nu_\tau$ decays and therefore could also be used to look for $\nu_e$ appearance in a predominantly $\nu_\mu$ beam by detecting their charged current (CC) interactions $\nu_e N \to e^- X$. The main motivation for this search was the evidence for $\bar{\nu}_\mu \to \bar{\nu}_e$ and $\nu_\mu \to \nu_e$ oscillations found by the LSND experiment [1]. For $\nu_\mu \to \nu_e$ oscillations with $\Delta m^2 \gtrsim 10$ eV$^2$ and with the probability of $2.6 \times 10^{-3}$ observed by LSND, a signal should be seen in the NOMAD data. The sensitivity of the NOMAD experiment to lower values of $\Delta m^2$ is limited by its $L/E_\nu$ ratio of $\sim 0.025$ km/GeV, where $L$ is the average source to detector distance and $E_\nu$ is the average neutrino energy.

Preliminary results of the search for $\nu_\mu \to \nu_e$ oscillations in NOMAD were presented earlier [2]. In this paper we report the final results of our "blind" analysis.

# 2 NOMAD detector and data collection

The NOMAD detector [3] consisted of a large dipole magnet delivering a field of 0.4 T and housing several subdetectors, starting with an active target composed of 132 planes of drift chambers (DC) of 3×3 m$^2$ [4]. The walls of the chambers provided a low average density (0.1 g/cm$^3$) target with a mass of 2.7 tons. The density of the chambers was low enough to allow an

---

[1] Deceased

3

accurate measurement of the momenta of the charged particles produced in the neutrino interactions. The chambers were followed by nine transition radiation (TRD) modules [5] each consisting of a polypropylene radiator and a plane of straw tubes operated with an 80% xenon and 20% methane gas mixture. An electromagnetic calorimeter (ECAL) consisting of 875 lead glass blocks [6,7] provided a measurement of the energies of electrons and photons with a resolution of $\sigma(E)/E = 3.2\%/\sqrt{E(\text{GeV})} + 1\%$. The ECAL was preceded by a lead-proportional tube preshower for better photon localization. A hadron calorimeter (HCAL) was located just beyond the magnet coil and was followed by two muon stations consisting of large area drift chambers, the first station located after 8, and the second one after 13 interaction lengths of iron. Two planes of scintillator counters, $T_1$ and $T_2$, were placed before and after the TRD modules. A third scintillator plane, $V$, placed upstream of the magnet, was used to veto interactions caused by incoming charged particles. The trigger [8] used in this analysis was $\bar{V} \times T_1 \times T_2$.

## 3  Neutrino beam

The CERN West Area Neutrino Facility (WANF) neutrino beam [9] was produced by impinging 450 GeV protons extracted from the SPS onto a target consisting of beryllium rods adding up to a total thickness of 110 cm. The secondary particles emerging from the target were focused into a near parallel beam by two magnetic lenses (the horn and the reflector) providing toroidal magnetic fields. When running in neutrino mode positively charged particles were focused. When running in the antineutrino mode the polarity of the two lenses was reversed thus focusing negatively charged particles. The focused particles then traversed a 290 m long decay tunnel followed by an iron and earth shield. Neutrinos originating from the decay of these particles travelled on average a distance of 625 m before reaching the NOMAD detector.

Since the oscillation search implies a direct comparison between the measured and expected ratios of the number of $\nu_e$ CC to $\nu_\mu$ CC interactions, an accurate prediction of the neutrino fluxes and spectra is crucial. They are computed with a detailed Monte Carlo simulation of the neutrino beam, referred to as NUBEAM and described in Ref. [10]. This is implemented in three steps. First, the yields of the secondary particles from the interactions of 450 GeV protons with the Be target are calculated with the 2000 version of FLUKA [11], a generator of hadronic interactions. These yields are then modified in order to agree with all measurements currently available in the relevant energy and angular range, namely the SPY/NA56 [12] and NA20 [13] results. Finally, the propagation of the secondary particles is described by a simulation program based on GEANT3 [14], which includes an accurate description of the magnetic
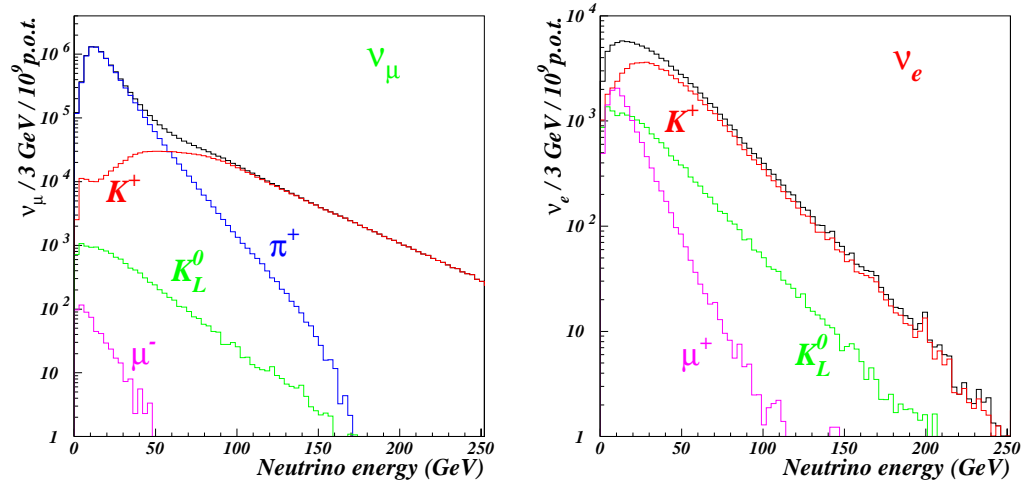
4

Fig. 1. Composition of the $\nu_\mu$ and $\nu_e$ energy spectra at NOMAD, within a transverse fiducial area of $260 \times 260$ cm$^2$, as predicted by the NOMAD simulation of the neutrino beam line.

field in the horn and reflector, and the modelling of reinteractions in the beam elements.

The resulting energy spectra of $\nu_\mu$ and $\nu_e$, and of their components, are shown in Fig. 1. The $\nu_\mu$ flux is predominantly due to decays of $\pi^+$ up to 60 GeV neutrino energy and to those of $K^+$ beyond this energy. The bulk of the $\nu_e$ flux comes from the decays of $K^+$, with $K^0_L$ contributing at the level of about 18% and $\mu^+$ at the level of about 14%. The composition of the beam is shown in Table 1.

Table 1
Average energies and relative abundances of the fluxes and charged current events of the four principal neutrino flavours at NOMAD, within a transverse fiducial area of $260 \times 260$ cm$^2$.

| Flavour | Flux | | CC interactions | |
| | $\langle E_\nu \rangle$ [GeV] | Rel. abund. | $\langle E \rangle$ [GeV] | Rel. abund. |
|---|---|---|---|---|
| $\nu_\mu$ | 24.3 | 1.0 | 47.5 | 1.0 |
| $\bar{\nu}_\mu$ | 17.2 | 0.068 | 42.0 | 0.024 |
| $\nu_e$ | 36.4 | 0.010 | 58.2 | 0.015 |
| $\bar{\nu}_e$ | 27.6 | 0.0027 | 50.9 | 0.0015 |

An alternative method of predicting the $\nu_e$ content of the beam, not used in this paper, has also been studied. This method, referred to as the Empirical Parameterization, does not use hadronic interaction packages such as FLUKA to predict the yield of particles from p-Be interactions. Instead it uses the $\nu_\mu$ CC, $\bar{\nu}_\mu$ CC and $\bar{\nu}_e$ CC events observed in NOMAD as well as the results of

5

NA20 and NA56 to constrain the hadron production cross sections, and using these, to predict the $\nu_e$ content of the beam.

## 4  Event simulation

The neutrino flux generated by NUBEAM was used as an input to the NO-MAD event generator to produce interactions of $\nu_\mu$, $\bar{\nu}_\mu$, $\nu_e$ and $\bar{\nu}_e$. Deep-inelastic scattering (DIS) events were simulated with a modified version of the LEPTO 6.1 event generator [15], with $Q^2$ and $W^2$ cutoffs removed. Quasi-elastic (QEL) [16] and resonance production (RES) [17] events were generated as well. The GRV-HO parameterization [18] of the parton density functions and the nucleon Fermi motion distribution of Ref. [19], truncated at 1 GeV/$c$, were used along with JETSET 7.4 [20] to treat the fragmentation.

The secondary particles produced in these interactions were then propagated through a full GEANT3 [14] simulation of the detector. The size of the simulated samples exceeded the data samples by about a factor of three for $\nu_\mu$ CC, 10 for $\bar{\nu}_\mu$ CC and neutral current (NC) and 100 for $\nu_e$ CC interactions.

The contributions of QEL, RES and DIS events in the Monte Carlo were adjusted to reproduce the $W^2$ distribution of $\nu_\mu$ CC interactions observed in the data, taking into account the non-isoscalarity of the NOMAD target (52.4% protons and 47.6% neutrons). The fractions of QEL and RES events included in the Monte Carlo are listed in Table 2.

Table 2
Estimated percentages of QEL and RES events in the NOMAD data.

| $\nu_\mu$ | | $\bar{\nu}_\mu$ | | $\nu_e$ | | $\bar{\nu}_e$ | |
|---|---|---|---|---|---|---|---|
| QEL | RES | QEL | RES | QEL | RES | QEL | RES |
| 2.5% | 3.3% | 6.3% | 7.1% | 1.7% | 2.2% | 4.3% | 4.8% |

## 5  Data collection and analysis

NOMAD collected data from 1995 to 1998. Most of the running, a total exposure of $5.1 \times 10^{19}$ protons on target (pot), was in neutrino mode and yielded $1.3 \times 10^6$ $\nu_\mu$ CC interactions in the fiducial volume of the detector. Some data, amounting to $0.44 \times 10^{19}$ pot, were also collected in antineutrino mode and some, $0.04 \times 10^{19}$ pot, in zero-focusing mode (with the horn and reflector switched off); these data were used mostly to check the beam simulation.

The trajectories of charged particles are reconstructed from the hits in the drift chambers and, from these trajectories, momenta are computed using the Kalman filter technique [21], which accounts for energy loss along the trajectory. As a first step the energy loss model used is that for pions, resulting in a momentum estimate, $p_\pi$, at the beginning of the track. Particles later identified as electrons or positrons are refitted [22] with an additional average energy loss due to bremsstrahlung, resulting in a new estimate, $p_e$, of the momentum. Energy clusters in the ECAL not associated to charged particles are assumed to be due to photons.

Vertices are reconstructed from the trajectories of charged particles. The energy of the incident neutrino, $E_\nu$, is approximated by the total (visible) energy of an event computed from the sum of the energies of all observed primary particles and of photons. The reconstruction efficiency for the hadronic jet was found to be overestimated by the Monte Carlo. This was due mostly to reconstruction effects such as the density cut described in Section 7, as well as an inadequate treatment of nuclear reinteractions (the interactions of produced particles inside the nucleus in which the neutrino interaction occurred) and a harder fragmentation in the Monte Carlo than observed in the data. The resulting overestimate of the scale of the hadronic energy, $E_h$, could be studied by noting that the differential cross section for charged current neutrino interactions is almost independent of $Y_{\mathrm{Bj}} = E_h/E_\nu$. This entails that the distribution of $R_E$, the ratio of the average neutrino energy in the data to the average neutrino energy in the Monte Carlo, will be independent of $Y_{\mathrm{Bj}}$ if $E_h$ is correctly measured. However, if the measured $E_h$ is systematically reduced by an amount $\alpha$ with respect to the true value of $E_h$, then the dependence of $R_E$ on $Y_{\mathrm{Bj}}$ can be described by a straight line with slope $(1 - \alpha)$ for small values of $\alpha$. Fitting the $R_E$ distribution as a function of $Y_{\mathrm{Bj}}$ allowed us to determine that the correction to $E_h$ is $\alpha = (8.3 \pm 1.5)\%$.

Since the electron radiates bremsstrahlung photons in traversing the drift chambers, in order to have an accurate measure of its energy, these photons must be identified and their energy added to the energy of the ECAL cluster at the end of the electron trajectory. Because of the curvature of the electron trajectory in the magnetic field these photons are located in a vertical fan delimited, on the one hand, by the actual trajectory of the electron between the event vertex and the point of impact of the electron on the ECAL and, on the other hand, by the extrapolation of the initial direction of the electron to the ECAL. The energy of photons in the ECAL and of photon conversions in the DC found in this region is included, resulting in a measure of the electron energy, $E_{\mathrm{brem}}$, with an average resolution of 2.1%.

# 6 Principles of oscillation search

The $\nu_\mu \to \nu_e$ oscillation signal should manifest itself as an excess in the number of $\nu_e$ CC events over that expected for an intrinsic $\nu_e$ contamination in the beam (about 1% of $\nu_\mu$). In order to reduce systematic uncertainties associated with absolute flux predictions and selection efficiencies, we study the ratio $R_{e\mu}$ of the number of $\nu_e$ to $\nu_\mu$ charged current interactions. Due to different energy and radial distributions of incident electron and muon neutrinos, the contribution of the intrinsic $\nu_e$ component is smaller at low $\nu_e$ energies, $E_\nu$, where a low $\Delta m^2$ oscillation signal is expected, and at small radial distances from the beam axis, $r$. Thus, the sensitivity of the search is increased by taking into account the dependence of $R_{e\mu}$ on $E_\nu$ and $r$.

The presence or absence of $\nu_\mu \to \nu_e$ oscillations is established by comparing the measured $R_{e\mu}$ with the one expected in the absence of oscillations. In order to avoid biases, we adopted a "blind analysis" strategy: the comparison of the measured to the predicted $R_{e\mu}$ is not made until the accuracy of the flux predictions and the robustness of the data analysis have been demonstrated and until all selection criteria are fixed. A number of control data samples in which no oscillation contribution is expected (charged current interactions of $\nu_\mu$, $\bar{\nu}_\mu$ and $\bar{\nu}_e$ in neutrino mode, and of $\nu_\mu$, $\bar{\nu}_\mu$, $\bar{\nu}_e$ and $\nu_e$ in antineutrino and zero-focusing modes) are used to verify the flux predictions and the validity of the Monte Carlo simulation [10]. It should be noted that no oscillation signal is expected to be measurable in $\bar{\nu}_e$ since the intrinsic ratio of $\bar{\nu}_\mu/\bar{\nu}_e$ in the beam is four times smaller than the intrinsic $\nu_\mu/\nu_e$ ratio and the antineutrino statistics is limited.

# 7 Event selection

In order to calculate $R_{e\mu}$, pure samples of $\nu_e$ CC and $\nu_\mu$ CC interactions are selected. The initial data sample for $\nu_e$ CC interactions is complementary to that used in the $\nu_\mu$ CC selection described below, i.e., it consists only of those events that include no muon (identified with looser criteria than in the $\nu_\mu$ CC selection). The basic requirement is the presence of a track associated with the neutrino interaction vertex, pointing to an energy deposition in the ECAL and identified as an electron in the TRD and ECAL. The identification criteria are:

– Pulse heights in the TRD consistent with those of an electron and such that isolated charged pions are rejected by at least a factor of 1000.
– A momentum-energy match satisfying:
  · $(E_{\text{brem}} - p_\pi)/(E_{\text{brem}} + p_\pi) > -0.3$;

· $(E_{\mathrm{brem}} - p_e)/(E_{\mathrm{brem}} + p_e) < 0.4$;
· no activity in HCAL associated with the electron trajectory.

Electrons from conversions and Dalitz decays are rejected by requiring:

– that the first point on the candidate track be within 15 cm of the primary vertex;
– that no positively charged track, either identified as a positron in the TRD or missing the TRD, when taken together with the candidate electron, results in the combination being consistent with a conversion. The criteria used are the invariant mass and the angle between the plane containing the trajectories of the two tracks and the vertical.

In order to reduce further the background from neutral current and charged current events in which the muon was not identified, kinematic cuts are also applied using the following two variables:

– $\phi_{\mathrm{eh}}$, the angle between the electron and the hadronic jet in the plane transverse to the neutrino beam direction.
– $Q_{\mathrm{lep}}$, the component of the electron momentum perpendicular to the hadronic jet direction.

Charged pions simulating secondary electrons and conversion electrons are part of the hadronic jet, resulting in small values of these variables. Primary electrons are isolated resulting in large values of $\phi_{\mathrm{eh}}$ and $Q_{\mathrm{lep}}$. These differences are evident in the $\phi_{\mathrm{eh}}$-$Q_{\mathrm{lep}}$ plots shown in Fig. 2 on which the cut used is also shown.

Single track events, originating mostly from quasi-elastic and resonance production interactions, are treated somewhat differently because they are more prone to background arising from charged particles entering the detector without being registered in the veto counter and because no hadronic jet containing primary charged particles is present. The criteria used to select them are:

– no activity in the drift chambers upstream of the beginning of the track and consistent with having given rise to the track;
– the angle between the single electron and neutrino beam directions, $\theta_{\nu e}$, smaller than 150 mrad;
– $Y_{\mathrm{Bj}} < 0.5$;
– $p_e \times \theta_{\nu e}^2 > 2m_e$, with $m_e$ the mass of the electron, a cut that rejects neutrino-electron scattering events.

Lastly, only events with $p_e > 2.5$ GeV/$c$ and $E_\nu < 300$ GeV are retained. These selection criteria result in an efficiency for $\nu_e$ CC, estimated from the Monte Carlo, of 43.9%.
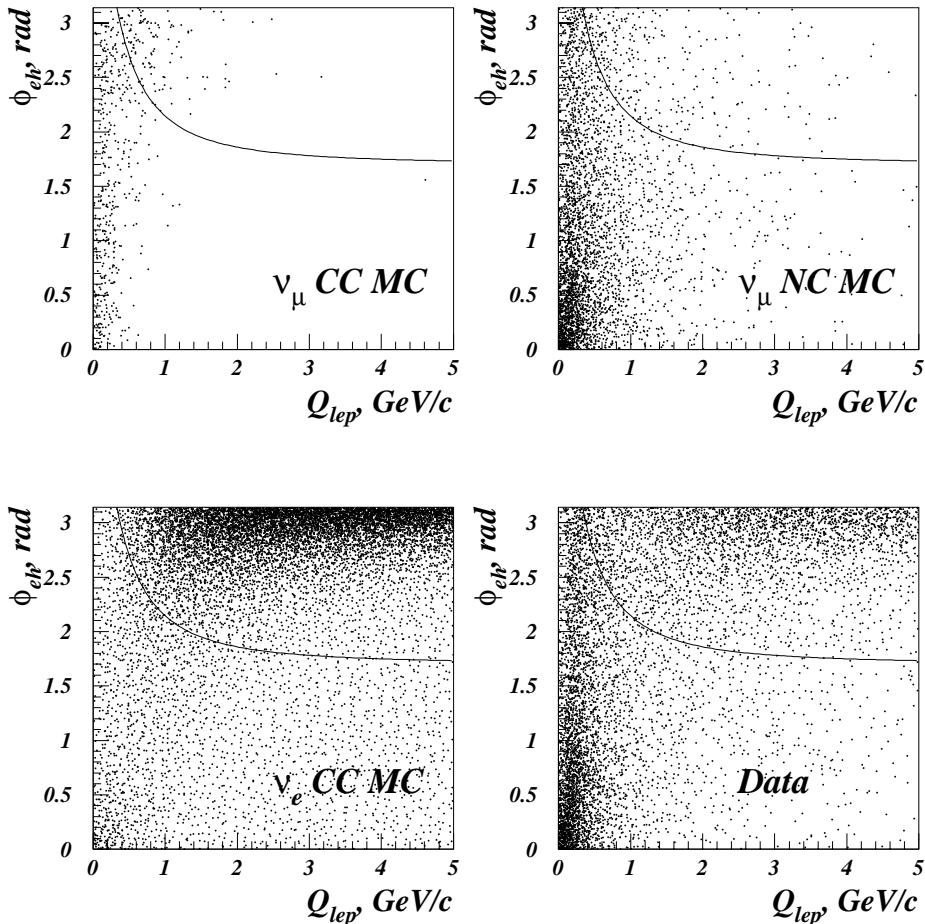
9

Fig. 2. The two-dimensional distributions $\phi_{eh}$-$Q_{lep}$ (defined in the text) for Monte Carlo $\nu_\mu$ CC and $\nu_\mu$ NC (background) events and for $\nu_e$ CC (signal) events, as well as for the NOMAD data. The events to the right of the curve were selected.

The surviving background contribution to the $\nu_e$ CC sample is estimated, from the Monte Carlo, to be 1.8%. It consists mostly of electrons from photon conversions. Their rejection depends critically on the reconstruction of the accompanying positron and on identifying a conversion point distinct from the primary vertex. The reconstruction of very low energy positrons and the separation of a conversion vertex from the primary vertex in a high multiplicity event could be different in the data and in the Monte Carlo. As a cross-check, a class of $e^+$ events that failed the kinematic cuts or were produced far from the primary vertex, and thus consisting almost entirely of background, were selected in both the data and in the Monte Carlo. The number of such events was found to be higher in the data by a factor that varied between 1.0 and 1.6 depending on $E_\nu$. The Monte Carlo background estimate for the $e^-$ events was therefore multiplied by this same factor, thus raising the total background estimate to 2.3%.

10
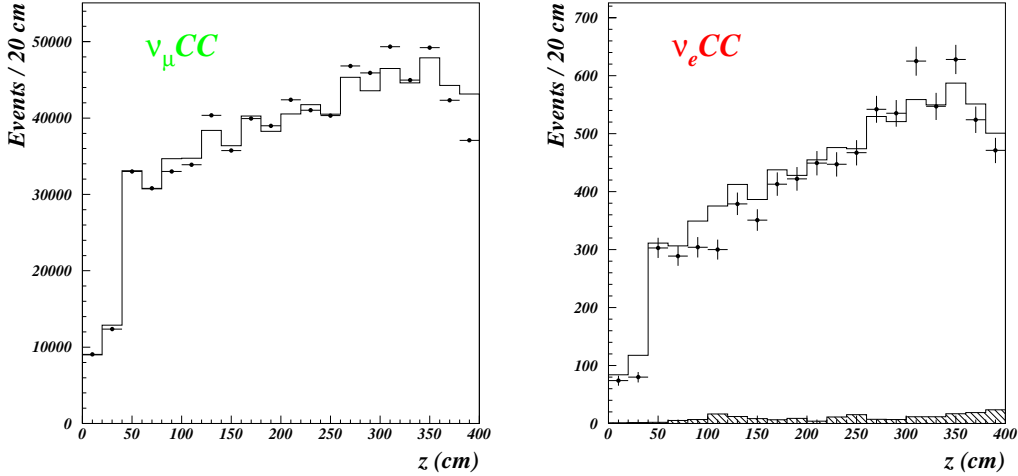
Fig. 3. The distributions of $z$ (defined in the text) for $\nu_\mu$ CC (left) and $\nu_e$ CC (right) candidates in the data (points with error bars) and in the Monte Carlo (histogram). The Monte Carlo distribution of $\nu_\mu$ CC events is normalized to the number of $\nu_\mu$ CC events in the data; the Monte Carlo distribution of $\nu_e$ CC events is normalized using the relative $\nu_e$ CC/$\nu_\mu$ CC abundance predicted by our simulation. The background contribution to the $\nu_e$ CC sample is shown in the hatched histogram.

Charged current interactions of $\nu_\mu$ are characterized by the presence of a primary muon in the final state, which had to penetrate 13 interaction lengths of absorber material to reach both muon stations in order to be identified. In addition, in order to minimize the differences between selection efficiencies of $\nu_\mu$ CC and $\nu_e$ CC events, we apply kinematic criteria identical to those used in the $\nu_e$ CC selection, although they are not needed for the background suppression. The resulting $\nu_\mu$ CC data sample has a negligible background contamination; the average selection efficiency is 60%.

The geometrical and kinematical distributions of both types of events are well reproduced by the Monte Carlo simulation, with the exception of the distribution of interaction vertices along $z$, the beam direction. The data and Monte Carlo $z$ distributions are shown in Fig. 3 for $\nu_\mu$ CC and $\nu_e$ CC events. It can be seen that fewer events are present in the data than in the Monte Carlo at small $z$ especially for $\nu_e$ CC events. The origin of this difference is due mostly to a cut introduced during the reconstruction of events: events with a very high density of hits in the drift chambers were not reconstructed due to a prohibitive reconstruction time. Since the data has on average a higher density of hits than the Monte Carlo, the effect of this cut is different on the two samples. Furthermore, since electrons radiate photons in traversing the drift chambers and some of these photons convert, the density of hits in $\nu_e$ CC events is large thus exacerbating the effect of the density cut for these events. The reprocessing of a sample of data and Monte Carlo events without this density cut resulted in $z$ distributions that were in much better
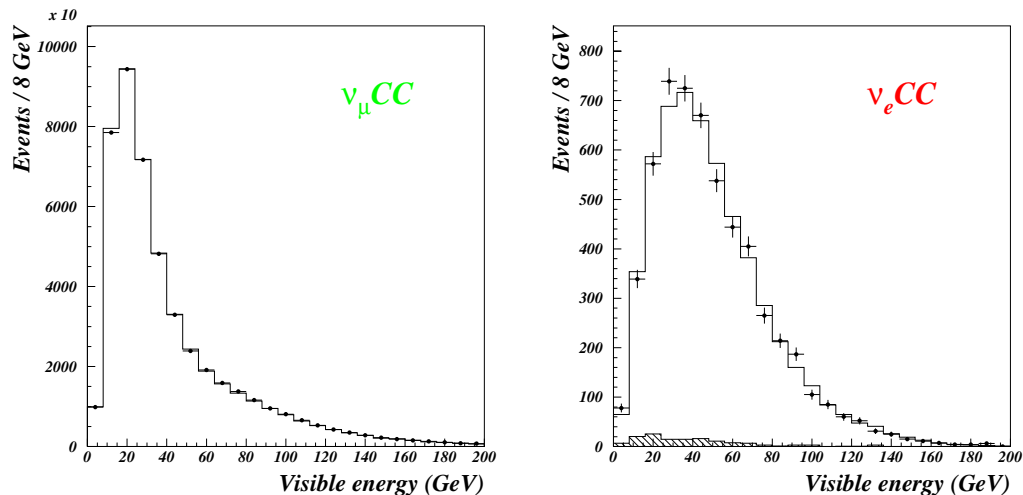
11

Fig. 4. Neutrino energy spectra for the data (points with error bars) and the Monte Carlo (histogram), for $\nu_\mu$ CC (left) and $\nu_e$ CC (right) candidates. The normalization of the Monte Carlo distributions is the same as in Fig. 3. The background contribution to the $\nu_e$ CC sample is shown in the hatched histogram.

agreement. We therefore decided to restrict the analysis to events occurring in the 72 downstream planes of drift chambers by requiring $z > 184$ cm. This restriction resulted in a loss of about 30% of the $\nu_e$ CC events and 35% of the $\nu_\mu$ CC events. It should be noted that any oscillation effects could not manifest themselves over this distance since the point of origin of the neutrinos is spread over more than 300 m.

A total of 5,584 $\nu_e$ CC and 472,378 $\nu_\mu$ CC events were retained. Their energy spectra and radial distributions are shown in Fig. 4 and Fig. 5, respectively.

## 8   Systematic uncertainties

The single largest uncertainty in this oscillation search is the uncertainty in the prediction of the fraction and the energy spectrum of intrinsic $\nu_e$ present in the beam. The computation of this uncertainty is described in detail in Ref. [10]. Most of it is due to the limited knowledge of the particle production cross sections in p-Be interactions. In turn, this is due to the small number of experimental data points on $\pi^+$ and $K^+$ production measured by NA20 and NA56, especially at non-zero values of transverse momentum. This uncertainty is energy-dependent; its typical fractional value at low $E_\nu$ is 4%. The second largest systematic error of about 3% comes from an uncertainty in the production of $K_L^0$ which accounts for 18% of the $\nu_e$ flux. Other potential sources of errors (such as tertiary particle yields, variations in the horn current, misalignments of the focusing devices and collimators, or inaccuracies in the
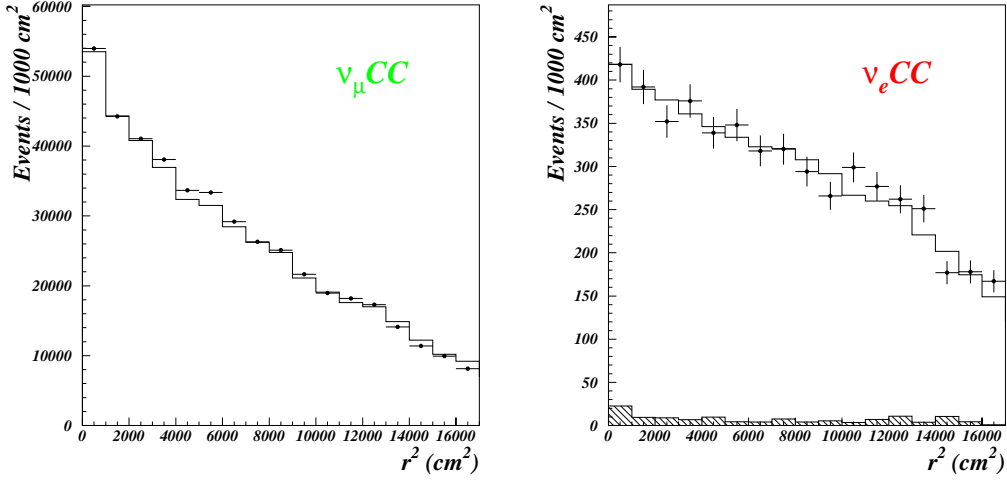
Fig. 5. The distribution of $r^2$, the square of the radial position of the neutrino interaction vertex with respect to the nominal beam axis, for the data (points with error bars) and the Monte Carlo (histogram), for $\nu_\mu$ CC (left) and $\nu_e$ CC (right) candidates. The normalization of the Monte Carlo distributions is the same as in the two previous plots. The background contribution to the $\nu_e$ CC sample is shown in the hatched histogram.

simulation of the beam line elements) have also been investigated [10]; their cumulative contribution is about 3%. The overall uncertainty arising from the knowledge of the beam composition is divided into an energy-independent, or normalization, uncertainty and an energy-dependent one. The normalization uncertainty on $R_{e\mu}$ is 4.2%, while the energy-dependent uncertainty, shown in Fig. 6, varies from 4% to 7%.
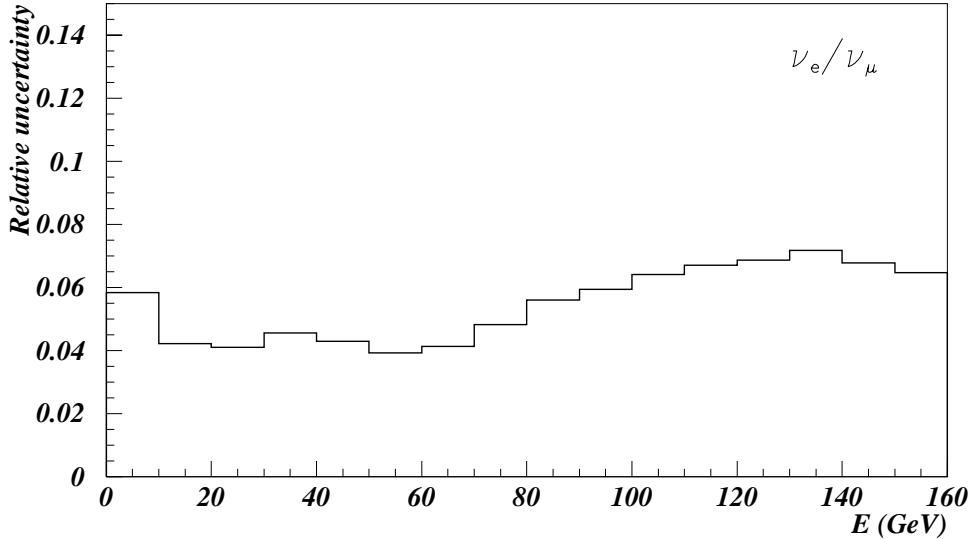


Fig. 6. Energy-dependent uncertainty in the prediction of the $R_{e\mu}$ ratio.

13

The following additional sources of systematic uncertainties arising from the data selection and analysis were studied:

– The correction to the background contribution. By studying the $e^+$ events used to determine this correction, the uncertainty attached to it was found to be 15%, resulting in an uncertainty of less than 1% in $R_{e\mu}$.

– The electron reconstruction and identification. The electron reconstruction efficiency in the drift chambers ($\sim 98\%$) was studied by defining electron tracks using the TRD, preshower and ECAL only, and then computing the frequency that a DC track is associated to the electron track. The electron identification efficiency of the TRD ($\sim 93\%$) was studied using $\delta$-rays produced by isolated muons arising from a nearby test beam and traversing the NOMAD detector outside of the neutrino spill. The efficiency of the momentum-energy consistency check was studied using $e^\pm$ from photon conversions. Taken together, the uncertainties in the reconstruction and identification efficiencies for electrons result in a 1% uncertainty in $R_{e\mu}$.

– A possible relative shift between the electron and muon energy scales. The upper limit on the absolute energy uncertainty of the ECAL was 0.5% [7], resulting in an uncertainty of less than 1% in $R_{e\mu}$. Non-linearity corrections to the ECAL energy scale have negligible effects on $R_{e\mu}$. The muon momentum scale introduced a negligible error.

– The mixture of QEL, RES and DIS events in the Monte Carlo. Cross sections for QEL and RES processes were varied by as much as 50% resulting in a negligible effect on $R_{e\mu}$.

– The fragmentation model. The effect on $R_{e\mu}$ of the fragmentation and nuclear reinteraction model used in the Monte Carlo was studied by comparing the prediction for $R_{e\mu}$ of two such models. Differences of up to 2% were observed and introduced as an energy-dependent systematic uncertainty.

– The kinematic (isolation) cuts. This was studied by tightening and loosening the cuts in both the data and Monte Carlo and studying the effect on $R_{e\mu}$. Since this was a blind analysis, this study could only be made after the analysis was frozen and the electron neutrino data examined. The effect was negligible in the relevant neutrino energy range, from 10 to 80 GeV.

– The hadronic energy scale. The 18% uncertainty on $\alpha$, the hadronic energy correction, resulted in less than a 1% uncertainty on $R_{e\mu}$ throughout the neutrino energy range. It was included as an energy-dependent uncertainty. The uncertainty arising from the method of calculating the hadronic energy was studied using two alternative methods to calculate it – the Myatt method [23] and the double-angle method [24], which use both the energy and direction of the lepton and only the direction of the hadronic jet. After computing the appropriate energy correction for each of these methods, no systematic differences were observed between these alternative methods and the method described in Section 5. Again, this study could only be performed after examining the electron data.

## 9  Results

The $R_{e\mu}$ distribution as a function of the visible energy obtained from the data is shown in Fig. 7, for the full radial acceptance (left) and in three radial bins (right). It is in good agreement with the Monte Carlo prediction under the no-oscillation hypothesis, also shown in the figure as $\pm 1\sigma$ uncertainty bands: a $\chi^2$ of 37.1/30 d.o.f. is obtained when the data are analyzed and compared to the simulation in the 10 energy bins and the 3 radial bins shown in Fig. 7 (incorporating both statistical and systematic uncertainties). The best fit to $\nu_\mu \rightarrow \nu_e$ oscillations, in the two-family approximation, gives a similar chi-squared value, $\chi^2_{\min} = 37.0/28$ d.o.f.
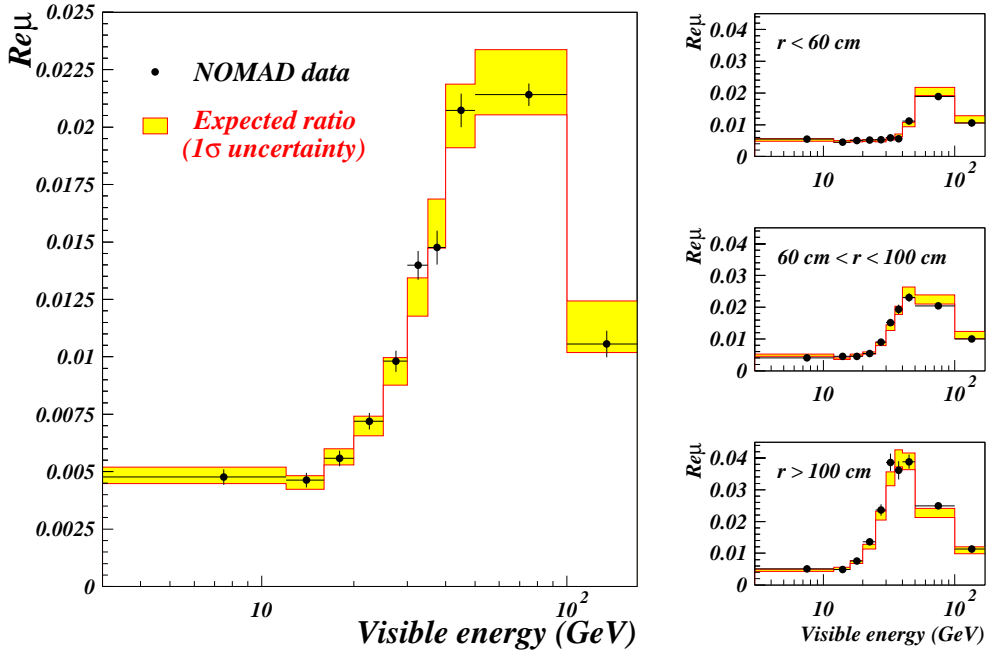


Fig. 7. The $R_{e\mu}$ ratio as a function of the visible energy for the data (points) and for the Monte Carlo prediction assuming no oscillations (filled bands), for the full radial acceptance (left) and in the three radial bins (right). The upper and lower boundaries of the bands correspond to the predictions with $\pm 1\sigma$ uncertainty, where $\sigma$ includes both the normalization and energy-dependent systematic uncertainties added in quadrature.

We use a frequentist approach [25] to set a 90% confidence upper limit on the oscillation parameters. The resulting exclusion region is shown in Fig. 8, together with results of other accelerator experiments, LSND [1], KARMEN [26], CCFR [27] and NuTeV [28], and the combined limit of Bugey [29] and Chooz [30] reactor experiments. Values of $\Delta m^2 > 0.4$ eV$^2$ for maximal mixing and $\sin^2(2\theta) > 1.4 \times 10^{-3}$ for large $\Delta m^2$ are excluded. For comparison, the sensitivity [25] of the experiment is found to be $\Delta m^2 > 0.4$ eV$^2$ for maximal

15
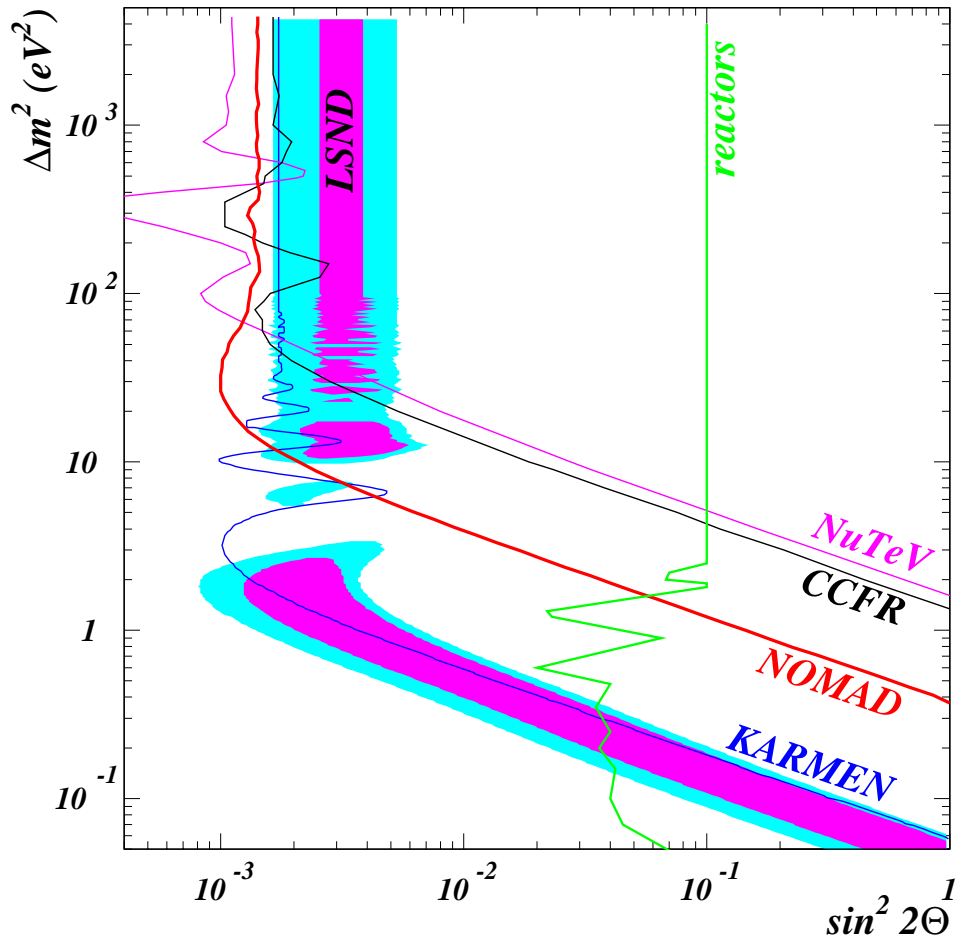
Fig. 8. The 90% C.L. exclusion region in the $\Delta m^2 - \sin^2(2\theta)$ plane from this analysis superimposed on the results of other experiments.

mixing and $\sin^2(2\theta) > 1.3 \times 10^{-3}$ at large $\Delta m^2$. Our result rules out the interpretation of the LSND measurements in terms of $\nu_\mu \rightarrow \nu_e$ oscillations with $\Delta m^2 \gtrsim 10$ eV$^2$.

This result is less stringent than our preliminary result [2] because of a better understanding of the systematic uncertainties arising from the knowledge of the beam composition. In particular, our previous analysis had underestimated the uncertainty arising from the $K^0_L$ contribution to the $\nu_e$ spectrum. In addition a different split between normalization and energy-dependent errors was implemented for the uncertainty arising from mesons produced in secondary interactions. After opening the box defined for the purpose of the blind analysis, no modifications were made either to the central value of the beam prediction or, other than the $z > 184$ cm cut described above, to the event selection procedure. We have ensured that including the events at $z < 184$ cm in the analysis did not alter our limit significantly.

# 10 Conclusion

The results of a search for $\nu_\mu \to \nu_e$ neutrino oscillations in the NOMAD experiment at CERN have been presented. The experiment looked for the appearance of $\nu_e$ in a predominantly $\nu_\mu$ wide-band neutrino beam at the CERN SPS. No evidence for oscillations was found. The 90% confidence limits obtained are $\Delta m^2 < 0.4$ eV$^2$ for maximal mixing and $\sin^2(2\theta) < 1.4 \times 10^{-3}$ for large $\Delta m^2$. This result excludes the high $\Delta m^2$ region of oscillation parameters favoured by the LSND experiment.

line.

## References

[1] LSND Collaboration,
C. Athanassopoulos et al., Phys. Rev. Lett. 77 (1996) 3082,
C. Athanassopoulos et al., Phys. Rev. Lett. 81 (1998) 1774,
A. Aguilar et al., Phys. Rev. D 64 (2001) 112007.

[2] V. Valuev, in: D. Horvath, P. Levai, A. Patkos, eds., *Proceedings of the EPS International Conference on High Energy Physics* (Budapest, Hungary, 2001), JHEP (http://jhep.sissa.it/) Proceedings Section, PrHEP-hep2001/190.

[3] NOMAD Collaboration, J. Altegoer et al., Nucl. Instrum. and Meth. A 404 (1998) 96.

[4] M. Anfreville et al., Nucl. Instrum. and Meth. A 481 (2002) 339.

[5] G. Bassompierre et al., Nucl. Instrum. and Meth. A 403 (1998) 363,
G. Bassompierre et al., Nucl. Instrum. and Meth. A 411 (1998) 63.

[6] D. Autiero et al., Nucl. Instrum. and Meth. A 372 (1996) 556,
D. Autiero et al., Nucl. Instrum. and Meth. A 373 (1996) 358,
D. Autiero et al., Nucl. Instrum. and Meth. A 411 (1998) 285,
D. Autiero et al., Nucl. Instrum. and Meth. A 425 (1999) 188.

[7] D. Autiero et al., Nucl. Instrum. and Meth. A 387 (1997) 352.

[8] J. Altegoer et al., Nucl. Instrum. and Meth. A 428 (1999) 299.

[9] G. Acquistapace et al., CERN-ECP 95-14, 1995.

[10] NOMAD Collaboration, P. Astier et al., "Prediction of neutrino fluxes in the NOMAD experiment", hep-ex/0306022, CERN–EP/2003–032, submitted to Nucl. Instrum. and Meth. A.

[11] A. Fassò, A. Ferrari, P.R. Sala and J. Ranft, in: A. Kling, F. Barao, M. Nakagawa, L. Tavora, P. Vaz, eds., *Proceedings of the Monte Carlo 2000 Conference* (Springer-Verlag, Berlin, 2001), 955.

[12] SPY Collaboration, G. Ambrosini et al., Eur. Phys. J. C 10 (1999) 605.

[13] H.W. Atherton et al., CERN Yellow Report 80-07, 1980.

[14] R. Brun, F. Carminati, GEANT Detector Description and Simulation Tool, CERN Program Library Long Writeup W5013, 1993.

[15] G. Ingelman, in: W. Buchmüller, G. Ingelman, eds., *Proceedings of the HERA Workshop* (DESY, Hamburg, 1992), 1336.

[16] C.H. Llewellyn Smith, Phys. Rep. 3 (1972) 261.

[17] D. Rein and L.M. Sehgal, Annals Phys. 133 (1981) 79.

[18] M. Glück, E. Reya, A. Vogt, Z. Phys. C 53 (1992) 127.

[19] A. Bodek, J. Ritchie, Phys. Rev. D 23 (1981) 1070.

[20] T. Sjöstrand, Comput. Phys. Commun. 39 (1986) 347;
T. Sjöstrand, M. Bengtsson, Comput. Phys. Commun. 43 (1987) 367;
T. Sjöstrand, Comput. Phys. Commun. 82 (1994) 74.

[21] R. Frühwirth, "Application of Filter Methods to the Reconstruction of Tracks
and Vertices in Events of Experimental High Energy Physics", HEPHY-PUB-
88-516, Vienna, 1988.

[22] P. Astier et al., Nucl. Instrum. and Meth. A 450 (2000) 138.

[23] G. Myatt, CERN/ECFA 72-4, Vol. II (1973) 117.

[24] S. Bentvelsen, J. Engelen and P. Kooijman, in: W. Buchmüller, G. Ingelman,
eds., *Proceedings of the HERA Workshop* (DESY, Hamburg, 1992), 23.

[25] G.J. Feldman, R.D. Cousins, Phys. Rev. D 57 (1998) 3873. See Sec. V.B.
For $\chi^2$, we use a Gaussian approximation with correlations; see Eqn. 31.14
in Review of Particle Properties, K. Hagiwara et al., Phys. Rev. D 66 (2002)
010001. The normalization uncertainty contributed fully correlated terms in
the covariance matrix; the energy-dependent uncertainties contributed terms
uncorrelated between different energy bins but fully correlated between radial
bins having common energies.

[26] KARMEN Collaboration, B. Armbruster et al., Phys. Rev. D 65 (2001) 112001.

[27] CCFR Collaboration, A. Romosan et al., Phys. Rev. Lett. 78 (1997) 2912.

[28] NuTeV Collaboration, S. Avvakumov et al., Phys. Rev. Lett. 89 (2002) 011804.

[29] B. Achkar et al., Nucl. Phys. B 434 (1995) 503.

[30] M. Apollonio et al., Eur. Phys. J. C 27 (2003) 331.